Supporting Information

Single atom catalysts for triiodide adsorption and fast conversion for boosted performance in aqueous zinc-iodine batteries

Fuhua Yang [1,2] [†], Jun Long [3] [†], Jodie A. Yuwono [1†], Huifang Fei[2],Yameng Fan [4], Peng Li[5], Jinshuo Zou [1], Junnan Hao [1], Sailin Liu [1], Gemeng Liang [1], Yanqiu Lyu [1], Xiaobo Zheng [6], Shiyong Zhao [1*], Kenneth Davey [1], Zaiping Guo [1] *

[1] School of Chemical Engineering and Advanced Materials, The University of Adelaide, Adelaide, SA 5005, Australia.

[2] Helmholtz Institute Ulm (HIU), Helmholtzstrasse 11, D-89081, Ulm, Germany

[3] Shenzhen Geim Graphene Center, Tsinghua-Berkeley Shenzhen Institute & Tsinghua Shenzhen International Graduate School, Tsinghua University, Shenzhen 518055, China.

[4] Institute for Superconducting and Electronic Materials, School of Mechanical, Materials, Mechatronics and Biomedical Engineering, University of Wollongong, North Wollongong, NSW 2522, Australia.

[5] School of Science, RMIT University, Melbourne, VIC 3000, Australia.

[6] Department of Chemistry, Tsinghua University, Beijing 100084, China.

[†] These authors contributed equally to this work

Corresponding author: shiyong.zhao@adelaide.edu.au; zaiping.guo@adelaide.edu.au

Experimental methods

Preparation of single atom catalysts

Ketjen black EC-600JD, KB (2 g) was obtained from Fuel Cell Store, and was annealed at 400 °C in a muffle furnace for 2 h. The product was mixed with distilled water and ethanol solution (AR) (volume ratio 1:1) and stirred for 1 h. The resulting black-colour paste was transferred to an autoclave and heated at 160 °C for 24 h, dried at 80 °C for 24 h, and left for further treatment.

The g-C_3N_4 was synthesized *via* directly heating Melamine ($C_3H_6N_6$, Sigma, 20 g) at 550 °C (ramp rate = 10 °C min^{-1}) for 2 h and placed in a covered alumina crucible inside a muffle furnace.

Copper (II) chloride dihydrate ($CuCl_2$-$2H_2O$) and Cobalt (II) chloride hexahydrate($CoCl_2$-$6H_2O$) (3.5 mmol) was dissolved in 30 mL distilled water. The mixture was stirred at room temperature (RT) (22 °C) for 2 h. The treated KB (1 g) was added to the metal salt solution and stirred for 3 h at 80 °C. Black powder was obtained through freeze- drying and ground with g-C_3N_4 (500 mg) for 30 min.

The compound was annealed through a two-stage pyrolysis, namely, 1) from 20 to 650 °C at a ramping rate 10 °C min^{-1}, maintained at 650 °C for 30 min and, 2) from 650 to 800 °C at a ramping rate 5 °C min^{-1}, maintained at 800 °C for 1 h, in a tubular furnace under Argon flow for 1 h. The product was leached at 60 °C in 1 M HCl for 6 h to remove metal clusters. The black-colour product was noted SAMe@NKB. For reference, the KJ black after 400 °C and hydrothermal treatment, was annealed at the same condition but without metal salt and noted as NKB.

Characterization

The morphology of the as-prepared SAMe@NKB and cycled Zn electrodes was determined *via* field-emission scanning electron microscopy (FESEM, JEOL JSM-7500FA) and scanning transmission electron microscopy (STEM, JEOL JEM-ARM200F). Raman spectra were obtained from a Raman spectrometer (Horiba LabRam Evolution). For the separator, aqueous filter-membrane with a thickness of ~ 90 μm was used, SEM and Raman measurements were conducted on the cross-section

of the separator, which were stripped from the Zn-I$_2$ batteries following the first cycle.

To confirm the crystalline structure for Zn anode, X-ray diffraction measurements were carried out on a PANalytical X'Pert Pro X-ray diffractometer with Cu Kα radiation and scan rate of 5° min^{-1} applied during measurement. Inductively coupled plasma atomic emission spectroscopy (TJA RADIAL IRIS 1000, ICP-AES) was used to determine the mass content of the (different) metals. X-ray absorption spectroscopy (XAS) was performed at the XAS Beamline (12ID) at the Australian Synchrotron. With the beamline optics used (Si-coated collimating, and Rh-coated focusing mirror), the harmonic content of the incident X-ray beam was almost negligible. The samples were mixed with a cellulose binder using a mortar and pestle for ~ 30 min and pressed into pellets for the tests.

Both fluorescence and transmission spectra were recorded based on concentration of metal in each sample. All XAS data were processed using Athena software. UV-vis spectra were collected on a UV3600 instrument (Shimadzu, Japan). X-ray photoelectron spectroscopy (XPS) measurements were made on a VG Multilab 2000 (VG) photoelectron spectrometer using monochromatic Al Kα radiation under vacuum of 2 ×10^{-7} Pa, and prior to data collection a 50 s ion etching was applied to each sample.

Electrochemical evaluation

To prepare the cathode electrode, a mixture of SAMe@NKB and PTFE in mass ratio 9:1 was finely ground in deionized (DI) water to prepare a slurry that was directly pasted on carbon-cloth before it was dried in a vacuum-oven at a temperature of 60 ^{o}C overnight. The control sample, NKB cathode electrode, was prepared using this same method. The as-prepared cathode electrodes were cut into pieces for the battery assembly. The electrolyte used included catholyte and anolyte. Catholyte was prepared *via* dissolving 0.1 M I$_2$ and 1 M LiI in DI water, whilst anolyte was 0.5 M ZnSO$_4$ and 0.5 M Li$_2$SO$_4$ in DI water. Mass loading for iodine species is ~2 mg cm^{-2}.

CR 2032 type coin cells were used for electrochemical tests in which stainless-steel shims and battery springs were used as supports, and a glass-fibre membrane as separator. Battery assembly was carried out in an ambient environment at RT. Catholyte

1 was dropped on as-prepared cathode and anolyte was used to wet the separator. Zinc-

2 foil was used as anode to 'match' with the cathode electrode.

3   Cycling and rate performance for the Zn-I_2 cells were determined within a voltage

4 window of 0.5 to 1.6 V *vs* Zn^{2+}/Zn at differing current density on Neware battery-testers

5 (CT-4008T-5V-50mA-164, Shenzhen, China). Current density and capacity were

6 computed based on the mass of iodine element in the catholyte. Cyclic voltammetry on

7 Zn-I_2 batteries with NKB, SACo@NKG and SACu@NKB cathode was carried out on

8 a VMP-3 electrochemical workstation at a scan rate 1 mV s^{-1} within a voltage window

9 of 0.5 to 1.6 V *vs* Zn^{2+}/Zn. Activation energy, E_a, was computed *via* the Arrhenius

10 equation from measurement of resistance of the battery under differing temperature:

$$\frac{1}{R_{ct}} = Aexp(-\frac{E_a}{R_0T})$$

11   (S1)

12 where R_{ct} is the charge transfer resistance.

13

14 **Computational Methods**

15 Density functional theory (DFT) computations were performed *via* Vienna *ab initio*

16 Simulation Program (VASP) [1, 2]. The generalized gradient approximation (GGA) in

17 the Perdew-Burke-Ernzerhof (PBE) form and a cutoff energy of 500 eV for planewave

18 basis set were adopted [3]. A $3 \times 3 \times 1$ Monkhorst-Pack grid was used for sampling the

19 Brillouin zones at structure optimization [4]. The ion-electron interactions were

20 described by the projector augmented wave (PAW) method [5]. A vacuum space

21 exceeding 20 Å was used to avoid interaction between two periodic units. The

22 convergence criteria of structure optimization were chosen as the maximum force on

23 each atom < 0.02 eV/Å with an energy change < 1×10^{-5} eV. The DFT-D3 semi-

24 empirical correction was *via* Grimme's scheme [6].

25

26 DFT calculations reveal that there are multiple active sites in the SAC model used,

27 including SA-site (metal-site), N-sites and C-sites. The adsorption energy calculations

28 The adsorption energies are calculated using the following equations:

29 E_{ads} (ads) = E(SAC*ads) – E(SAC) – E(ads)

where E(SAC*ads) represents the electronic energy of SAC with adsorbate, E(SAC) is the electronic energy of clean SAC and E(ads) is the electronic energy of adsorbate, i.e., I_2, I_3 and I.

Whereas the free energy diagram for I_2 reduction as a function of potential (V *vs* Zn^{2+}/Zn) is calculated using the following mechanism:

$* + 1.5\ I_2 + 0.5\ Zn \rightarrow *I_2 + 0.5\ I_2 + 0.5\ Zn \rightarrow *I_3 + 0.5\ Zn \rightarrow *I + 2\ I_2 + 0.5\ Zn \rightarrow * + 0.5\ ZnI_2 + 2\ I_2$
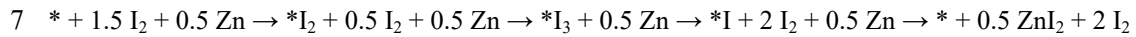
The symbol * here represent active site in SAC, which then is occupied by different intermediates during the reduction of I_2 to I^-. The formation of I^- as a final product in this reaction path is identified by the formation of ZnI_2.

References

[1]   G.Kresse, J. Furthmüller, Comput. Mater. Sci. 1 (1996) 15-50.

[2]   G.Kresse, J. Furthmüller, Phys. Rev. B. 16 (1996) 11169-11186.

[3]   J.P. Perdew, K. Burke, M. Ernzerhof, Phys. Rev. Lett. 18 (1996) 3865-3868.

[4]   H.J. Monkhorst, J.D. Pack, Phys. Rev. B. 13 (1976) 5188-5192.

[5]   P.E. Blöchl, Phys. Rev. B. 50 (1994) 17953-17979.

[6]   S. Grimme, J. Antony, S. Ehrlich and H. Krieg, J .Chem. Phys. 132 (2010) 154104.
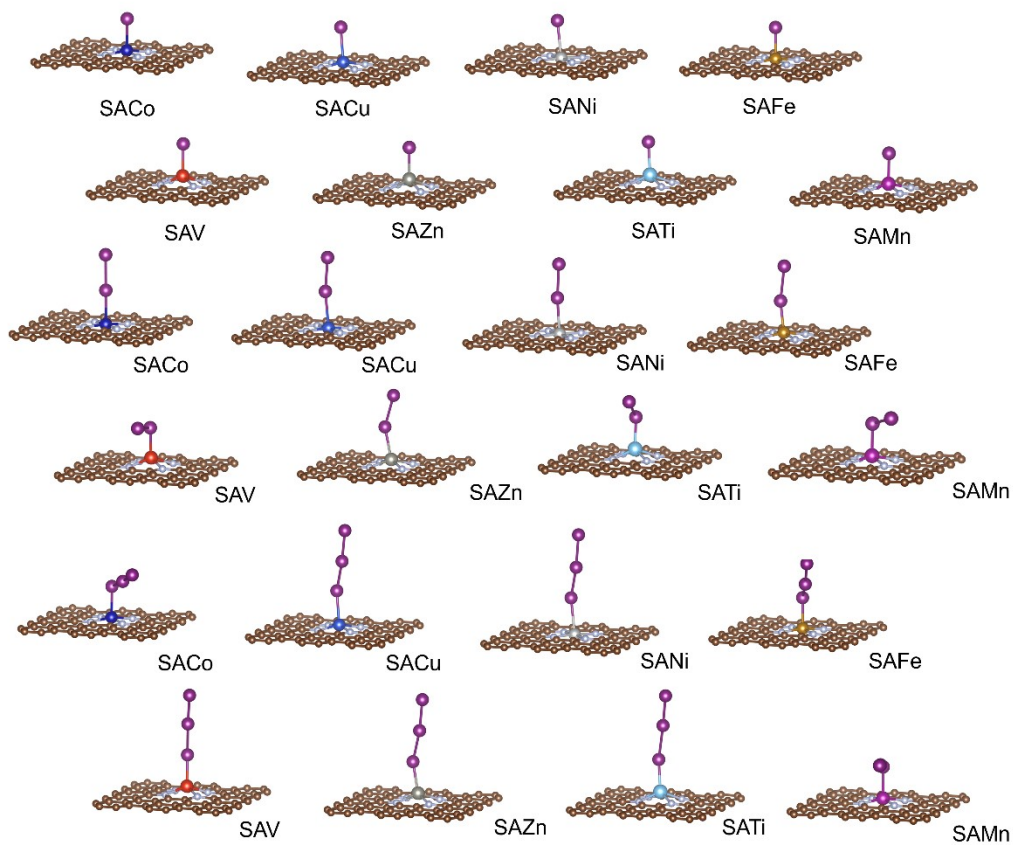
Figure S1. DFT-optimized models showing I_2 and intermediates adsorption on selected SACs@N-doped graphene (NG): SAC*I, SAC*I_2, SAC*I_3.

1
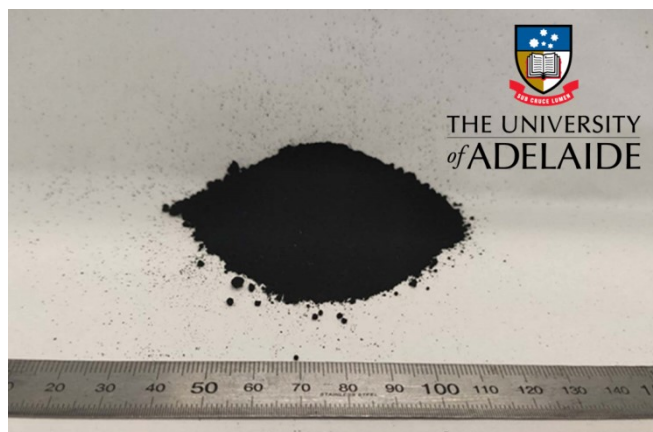
2

3

4 Figure S2. Photograph of 3 g SACu@NKB.
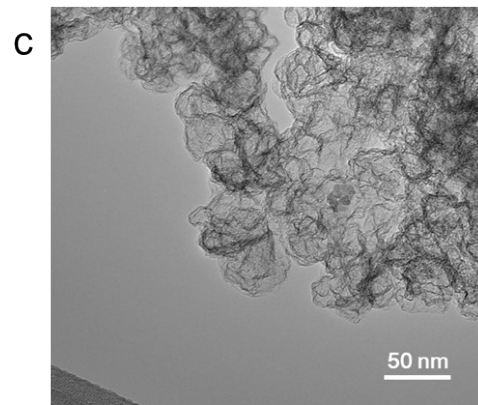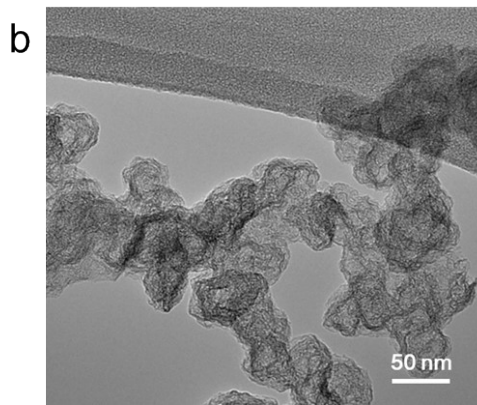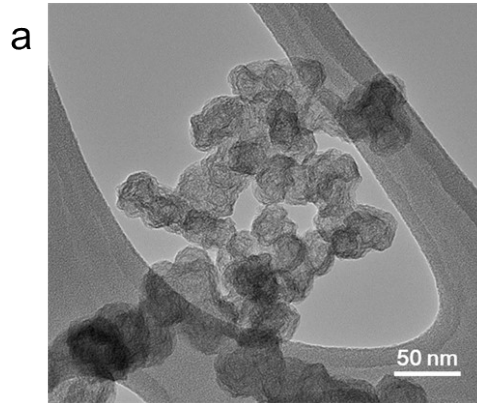
5

Figure S3. TEM image for a) NKB, b) SACo@NKB and c) SACu@NKB.
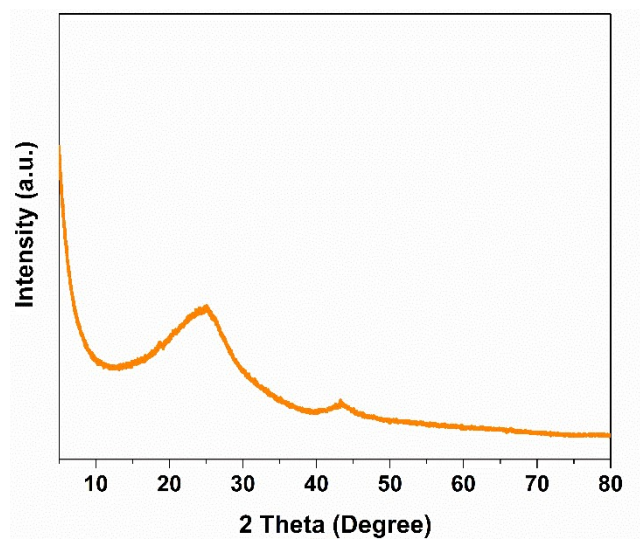
Figure S4. XRD pattern of SACu@NKB.
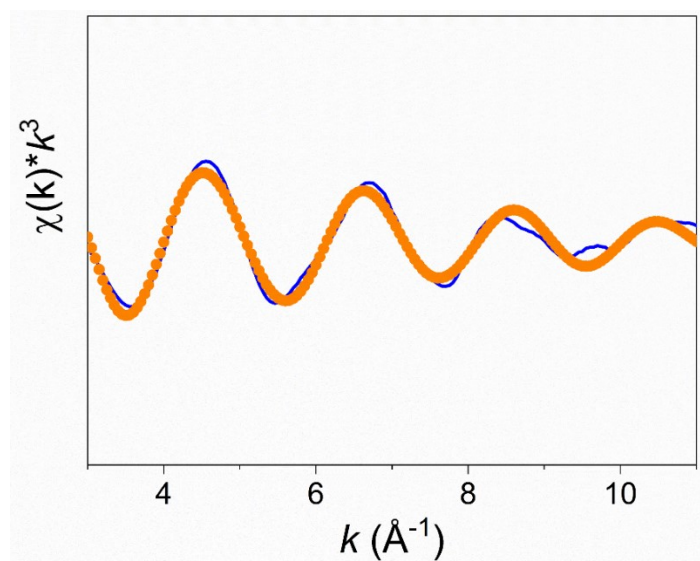
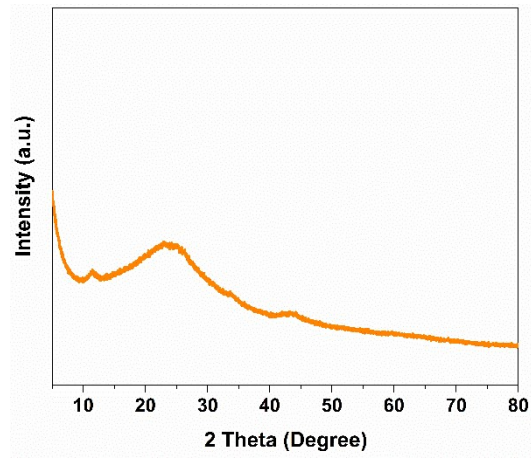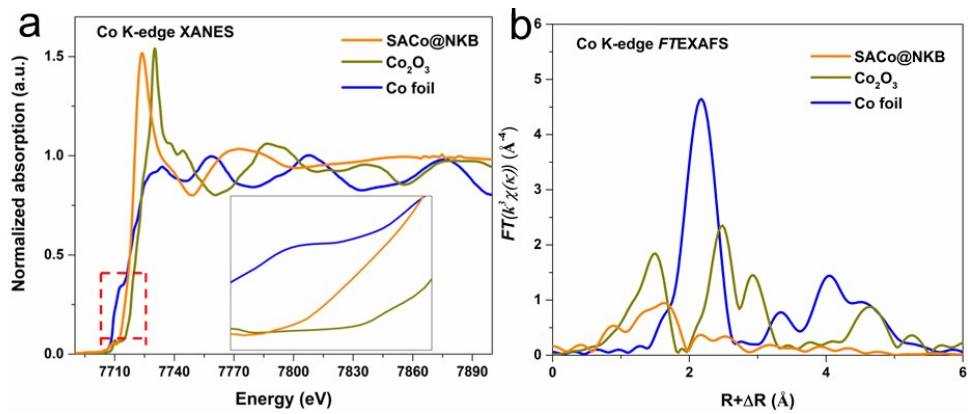Figure S5. k-space and the corresponding fitting results for SACu@NKB.
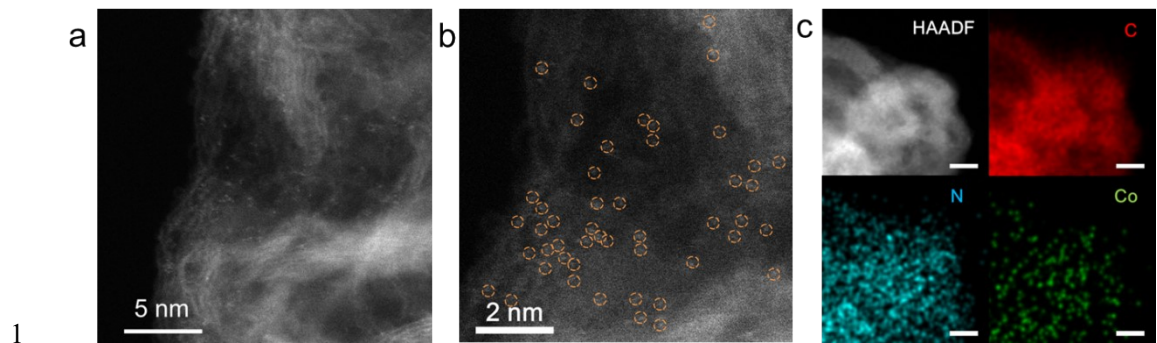
Figure S6. a) and b) Representative HAADF-STEM image of SACo@NKB. c) STEM-EDS elemental mapping for SACo@NKB. Scale bar = 5 nm.

1

2 Figure S7. XRD pattern of SACo@NKB.

3

Figure S8. a) Normalized Co K-edge XANES and b) FT-EXAFS spectra for SACo@NKB, Co-foil and Co$_2$O$_3$.
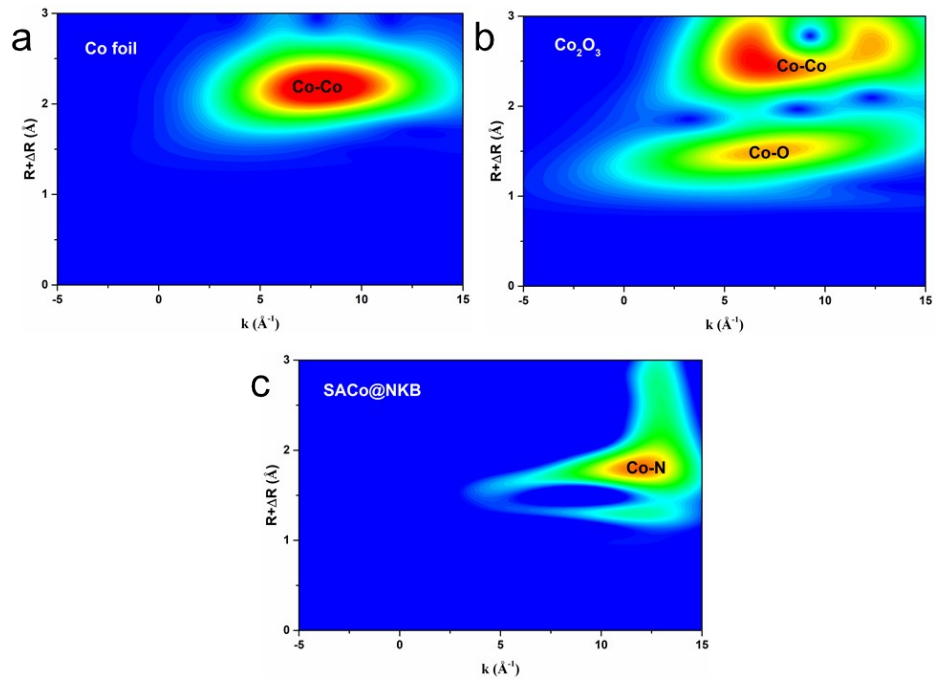
Figure S9. WT contour plots for Co K-edge at R space for a) Co-foil, b) Co_2O_3 and c) SACo@NKB.
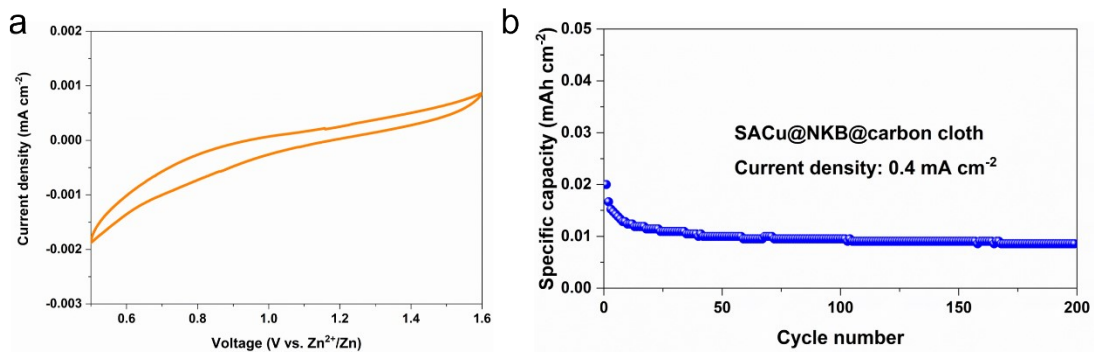
Figuer S10. (a) CV curves of SACu@NKB@carbon cloth within the tested voltage window of 0.5-1.6 V vs. Zn^{2+}/Zn at a scan rate of 0.2 mV s^{-1}. (b) Cycling performance of pure SACu@NKB@carbon cloth without the addition of catholyte at a current density of 0.4 mA cm^{-2}.

1
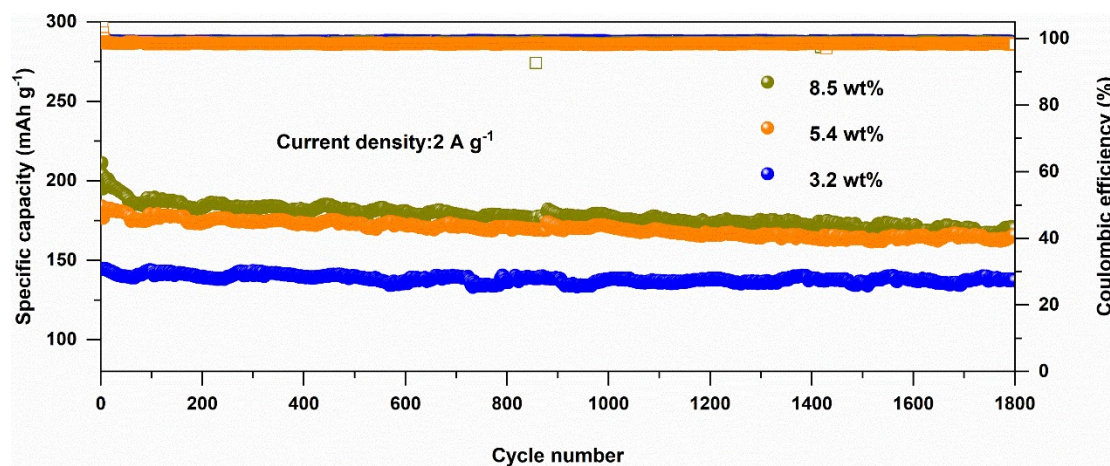
2
3 Figure S11. Cycling performance of SACu@NKB cathode with various SACu
4 contents.

1
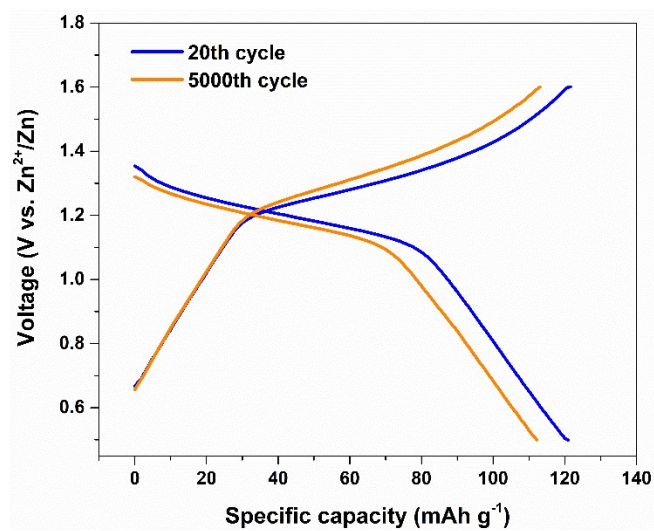
2

3

4 Figure S12. Charge-discharge curve for Zn-I$_2$ battery with SACu@NKB cathode at 20th
5 and 5000th cycle under current density 5 A g^{-1}.
6
7

1
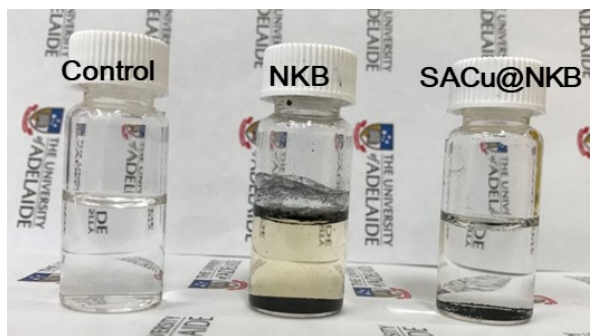
2
3
4 Figure S13. Photograph of mixture of NKB/triiodide and SACu@NKB/triiodide
5 immersed in DI water following one-week rest.
6

1

2
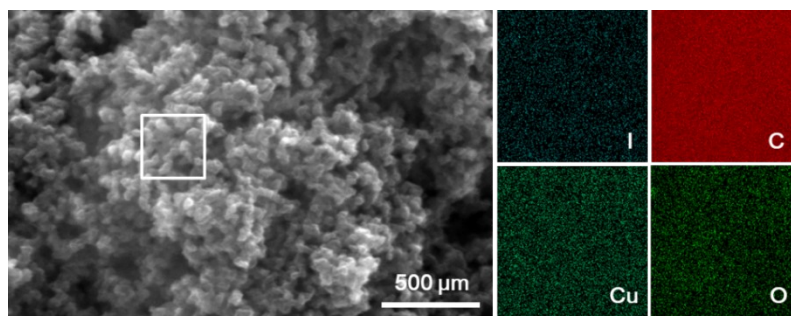
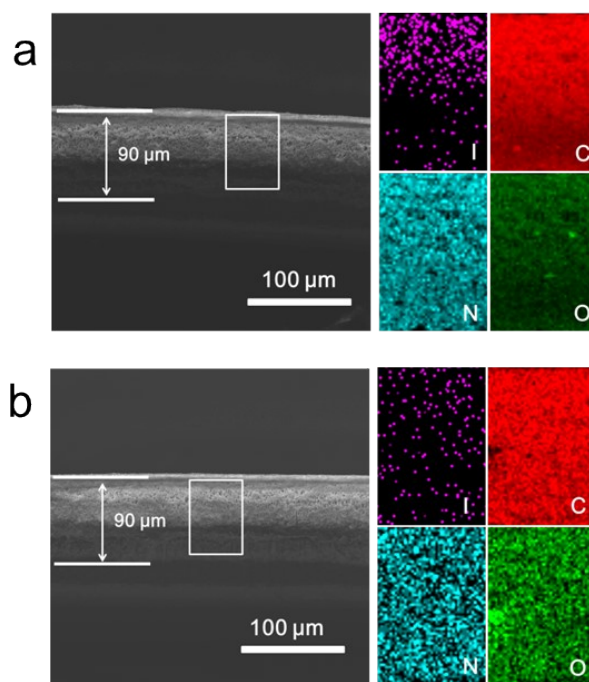3 Figure S14. SEM image of SACu@NKB/triiodide mixture and corresponding elements

4 mapping.

5
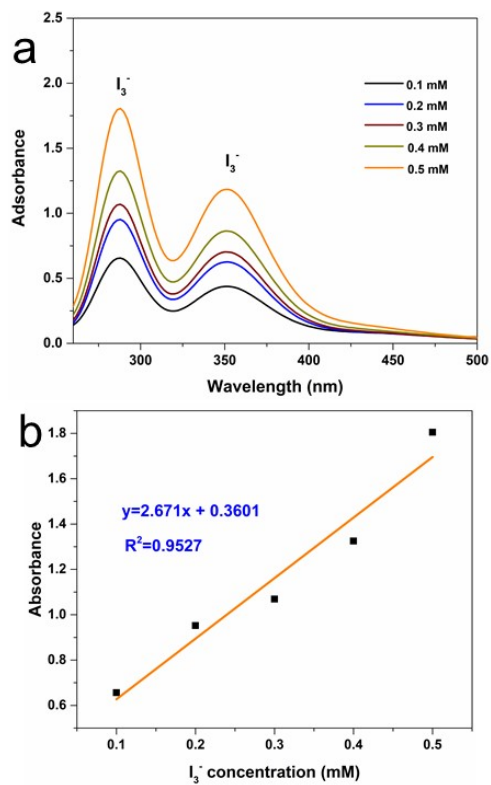
Figure S15. a) UV-vis spectra for triiodide solution with differing concentration. b) Corresponding working plots confirming the relationship between concentration and absorbance.

1
2
3 Figure S16. SEM image of cross-section of water filter paper separator from Zn-I$_2$
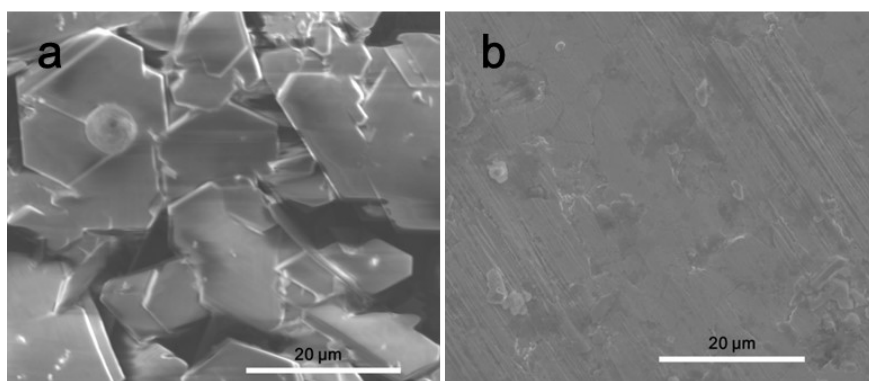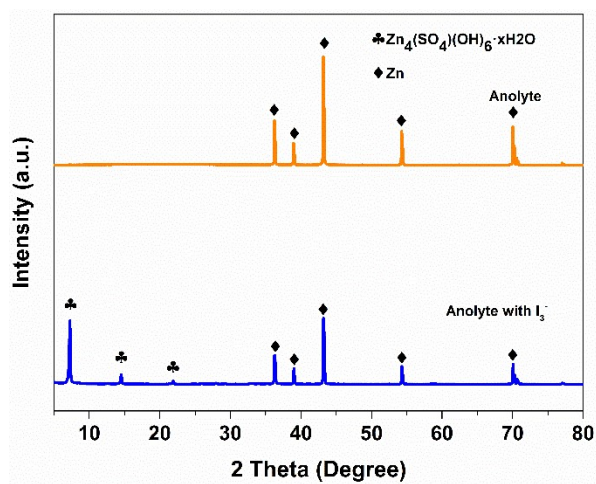4 battery with a) NKB and b) SACu@NKB, cathode and corresponding elements
5 mapping.
6
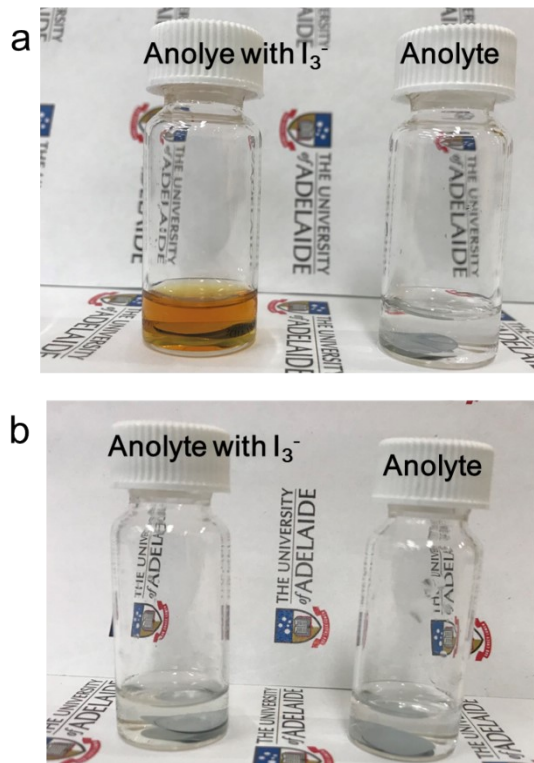
Figure S17. Identical Zn foils immersed in anodelyte with I_3^- solution and bare anodelyte a) prior to and b) following, one-week rest.

Figure S18. SEM image of Zn-foil following immersion in a) anodelyte with I_3^- solution and b) bare anodelyte, for one-week.
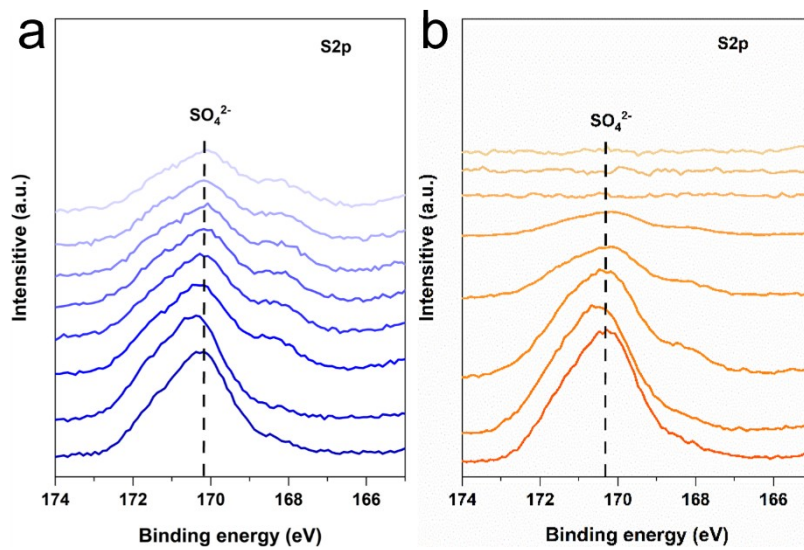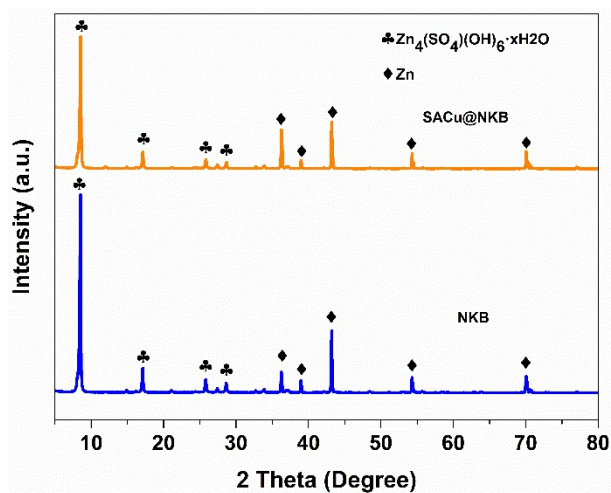
Figure S19. XRD pattern for Zn-foil following immersion in anodelyte with I_3^- solution and bare anodelyte, for one-week.

Figure S20. S2p XPS depth profiles for Zn anodes following 50 cycles in Zn-I$_2$ battery with a) NKB and b) SACu@NKB cathode.
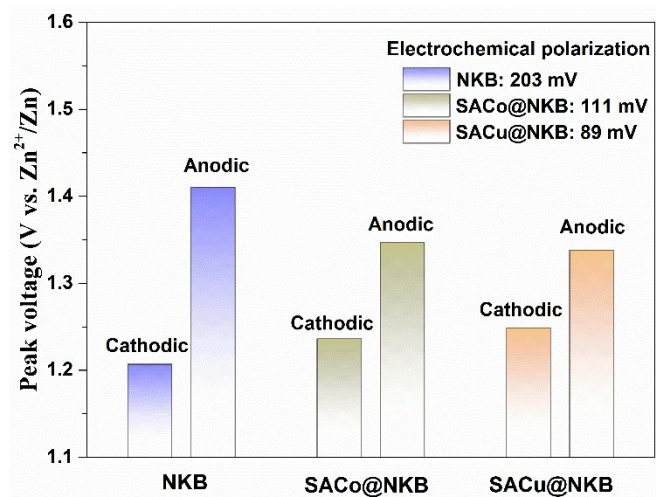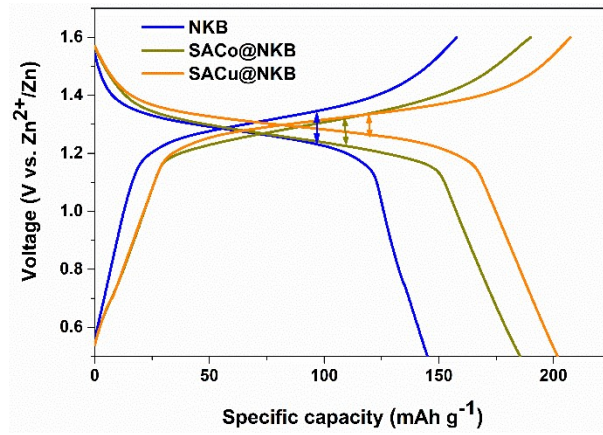
1

2

3

4 Figure S21. XRD pattern for Zn anode after 50 cycles in NKB-based Zn-I$_2$ battery and

5 SACu@NKB -based Zn-I$_2$ battery.

6

1
2 Figure S22. Peak potential for CV curves for Zn-I_2 batteries.
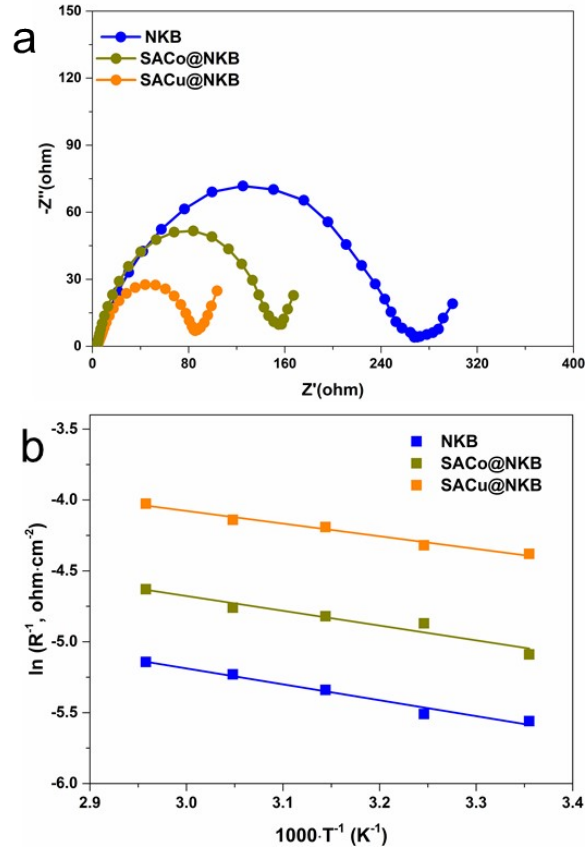3
4

Figure S23. Charge-discharge curve for Zn-I$_2$ batteries with NKB, SACo@NKB and SACu@NKB cathodes under current density 0.2A g^{-1}.
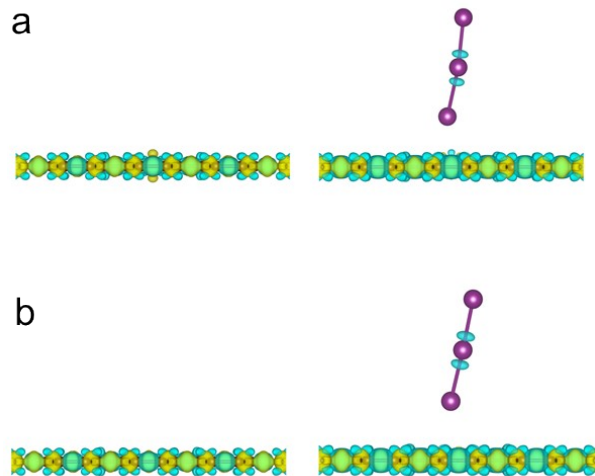
Figure S24. a) EIS measurement of Zn-I$_2$ batteries with NKB, SACo@NKB and SACu@NKB cathodes at 298 K. b) Arrhenius plot demonstrating linear relationship between log-reciprocal of charge transfer resistance and reciprocal of absolute temperature of Zn-I$_2$ batteries with NKB, SACo@NKB and SACu@NKB cathodes.

Figure S25. Side-view (elevation) of charge density distribution for (a) SACo and (b) SACu, prior to and following adsorption of $*I_3$.

1 **Supplementary Table 1**. EXAFS fitting parameters at the Cu K-edge for SACu

2 samples.

	Shell	N[a]	R (Å)[b]	σ2 (Å2)[c]	ΔE0 (eV)[d]	R factor
Cu SA	Cu-N	4 ± 0.8	1.95 ± 0.02	0.008	9.6 ± 2.3	1.5%

3
4
5
6 **END OF SI**
7
8